JACS
JOURNAL OF THE AMERICAN CHEMICAL SOCIETY
Article
pubs.acs.org/JACS

Molecular Switching via Multiplicity-Exclusive *E*/*Z* Photoisomerization Pathways

Jiawang Zhou,[†] Xin Guo,[‡,§] Howard E. Katz,[†,‡] and Arthur E. Bragg*[,†]

[†]Department of Chemistry, Johns Hopkins University, Baltimore, Maryland 21218, United States
[‡]Department of Materials Science and Engineering, Johns Hopkins University, Baltimore, Maryland 21218, United States

Supporting Information

ABSTRACT: Mutual exclusivity in the nature of forward and reserve isomerization pathways holds promise for predictably controlling responses of photoswitchable materials according to molecular structure or external stimuli. Herein we have characterized the *E*/*Z* photoisomerization mechanisms of the visible-light-triggered switch 1,2-dithienyl-1,2-dicyanoethene (4TCE) in chlorobenzene with ultrafast transient absorption spectroscopy. We observe that switching mechanisms occur exclusively by relaxation through electronic manifolds of different spin multiplicity: *trans*-to-*cis* isomerization only occurs via electronic relaxation within the singlet manifold on a time scale of 40 ps; in contrast, *cis*-to-*trans* isomerization is not observed above 440 nm, but occurs via two rapid ISC processes into and out of the triplet manifold on time scales of ∼2 ps and 0.4 ns, respectively, when excited at higher energies (e.g., 420 nm). Observation of ultrafast ISC in *cis*-4TCE is consistent with photoinduced dynamics of related thiophene-based oligomers. Interpretation of the photophysical pathways underlying these isomerization reactions is supported by the observation that *cis*-to-*trans* isomerization occurs efficiently via triplet-sensitized energy transfer, whereas *trans*-to-*cis* isomerization does not. Quantum-chemical calculations reveal that the T_1 potential energy surface is barrierless along the coordinate of the central ethylene dihedral angle (θ) from the *cis* Franck–Condon region ($\theta = 175°$) to geometries that are within the region of the *trans* ground-state well; furthermore, the T_1 and S_1 surfaces cross with a substantial spin–orbital coupling. In total, we demonstrate that *E*/*Z* photoswitching of 4TCE operates by multiplicity-exclusive pathways, enabling additional means for tailoring switch performance by manipulating spin–orbit couplings through variations in molecular structure or physical environment.

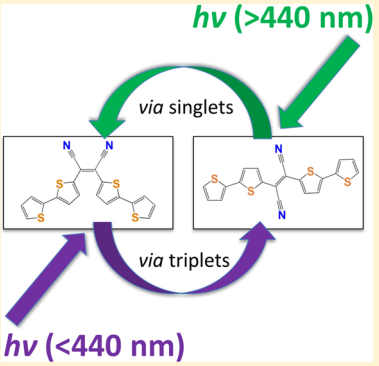

1. INTRODUCTION

Photoswitchable molecules and materials that exhibit substantial changes in structure or functional properties upon wavelength-selective excitation are of considerable interest for numerous applications,[1−3] including photochromism,[4] memory storage,[5] logic devices,[6] molecular motors,[7,8] mechanical manipulation,[9−13] and light-triggered chemical sensitization[14] and conductivity.[15] Photoswitches that operate via large-scale structural changes, such as *E*/*Z* isomerization, are particularly attractive for manipulating the distance between chemical or biochemical moieties to interrogate the nature of their interactions.[9−13,16−19] Photoswitching also has potential for controlling or patterning morphologies of aggregated organic materials.[20,21] Desirable photoswitch characteristics include high conversion efficiency,[22,23] robust fatigue resistance,[24] and the feasibility for isomerization at red excitation wavelengths[25−27] that can transmit through materials such as biological tissue.[9] In addition, mutual exclusivity in the nature of the excited-state relaxation pathways that drive forward and reserve isomerization reactions can provide a handle for controlling the reversibility of a switch as desired for a particular application.[28,29] On all counts, an understanding of photophysical dynamics and how they may be manipulated with structure are of prime importance for the synthetic design of photoresponsive materials.

Previously we reported a new photochromic molecule, a 1,2-dithienyl-1,2-dicyanoethene (4TCE), that can be induced to isomerize via excitation at visible wavelengths and that exhibits relatively high photostationary yields for photochromic conversion upon irradiation.[27] The UV–vis spectra and structures for both *cis* and *trans* isomers are shown in Figure 1. The *trans* isomer of 4TCE is most stable energetically when dissolved in solution at room temperature, but is readily converted to the more photostable *cis* isomer in 100% yield upon exposure to room lights. In contrast, the reverse process can be accomplished either through illumination with blue light (<440 nm, ∼60% photostationary conversion in toluene) or by heating (>80 °C, 100% conversion). All isomerization processes are complete in the course of minutes. Importantly, the low reactivity of the β carbon sites on the thiophene rings eliminates the possibility of a competing cyclization pathway at low energies, such that 4TCE is a two-state *E*/*Z* switch when used in conjunction with visible light. Additionally, 4TCE possesses high photostability, with no detectable photo-

Received: July 14, 2015
Published: August 10, 2015

DOI: 10.1021/jacs.5b07348
J. Am. Chem. Soc. 2015, 137, 10841−10850

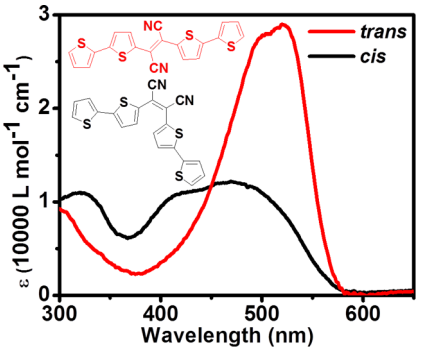

Figure 1. UV−vis absorption spectra of 4TCE isomers in chlorobenzene (CB) (2.4×10^{-5} M). The structures of *trans* and *cis* isomers of 4TCE are shown in the inset.

degradation after several isomerization cycles. A particularly attractive feature of the 4TCE switch design is that oligothienyl groups could be lengthened, affecting both photoswitchable mechanical separation of its two ends and the spectral properties of the switch; notably, longer pendant oligothienyl groups would give rise to increased molecular conjugation and a redder absorption spectrum.

We previously ascribed the photoswitching characteristics of 4TCE to the large separation in maximum absorption wavelength (λ_{max}) and differences in molar extinction coefficient (ε) between the *trans* and *cis* isomers (Figure 1): λ_{max} for the *trans* and *cis* isomers are located at 520 and 470 nm in toluene, and the ε of *trans* is 2.5 times larger than that of *cis* at their respective λ_{max}. However, a complete characterization of the relative photoselectivity for each of these pathways and their corresponding photostationary yields must also take into consideration the energy-dependent quantum yields for isomerization, which are determined by the nature of underlying photophysical processes. As small thiophene-based systems are known to exhibit large spin−orbit couplings (SOCs) and efficient intersystem crossing (ISC) rates in their excited states due to the presence of sulfur atoms,[30−35] the *E*−*Z* and *Z*−*E* isomerization reactions of 4TCE also might be expected to occur via electronic relaxation through either or both of the singlet and triplet manifolds; in contrast, *E*/*Z* switches such as stilbenes and azobenzenes only occur by way of singlet relaxation pathways upon direct photoexcitation.[12,36,37] Manifold-exclusive relaxation pathways could enable control of the relative significance of one pathway over the other by tailored molecular design, energy-transfer sensitization, or the application of external stimuli (e.g., electric fields). Thus, an understanding of photoswitching behavior and how to manipulate switch properties for improved performance or extended spectral utilization requires greater understanding of how molecular structure impacts the course of excited-state dynamics in either direction.

Toward this end, we have used ultrafast transient absorption (TA) spectroscopy to interrogate the relaxation pathways associated with the energy-dependent isomerization of 4TCE. We find that *trans*-to-*cis* isomerization occurs via relaxation only through singlet electronic states following low-energy excitation (530 nm); low-energy excitation of the *cis* isomer likewise results in electronic relaxation only via singlets, but with negligible isomerization. In contrast, transient spectral dynamics measured at higher excitation energies (420 nm) reveal that excited-state relaxation of both species and isomerization of the *cis* isomer, in particular, involves ISC into and out of the triplet manifold. As *cis* relaxation is driven by fast (~2 ps) and efficient ISC from the optically active singlet level, we hypothesize that structural modifications that enhance or disrupt spin−orbit couplings between manifolds could be used to manipulate *cis*-to-*trans* photostationary yields. We further demonstrate that triplet sensitization may provide an alternate method for highly pathway-selective *E*/*Z* isomerization of 4TCE and its derivatives at red wavelengths with high photostationary yield.

2. EXPERIMENTAL AND COMPUTATIONAL METHODS

2.1. Sample Preparation and Characterization. The synthesis of 4TCE has been described previously.[27] Solutions of 4TCE in chlorobenzene (CB, Fisher Scientific, >99% purity) were prepared at concentrations of ~2.4×10^{-5} mol/L. Sample solutions were circulated through a 1 mm path-length quartz flow cell for optical measurements. The optical density of the sample solutions were ~0.8 and ~0.3 for *trans* and *cis* at their peak absorption wavelengths, respectively. All components of the flow circuit are chemically resistant to sample solutions.

Exposure to room light can drive the isomerization from *trans* to *cis* in solution to completion, and therefore spectroscopic measurements of *trans*-to-*cis* isomerization were conducted in the absence of room light. In contrast, the pure *trans* form of 4TCE can be prepared by heating a *cis* or mixed *cis*/*trans* sample to 80 °C and then cooling it to room temperature in the dark. These processes were used to purify samples before laser experiments.

A diode-array spectrometer fiber-optically coupled to tungsten and incandescent deuterium light sources (Stellarnet) was used to measure steady-state UV−vis spectra of sample solutions before and after time-resolved measurements. For measurements of *trans* to *cis* isomerization, no noticeable change of the *trans* ground state absorption was observed, indicating that the amount of *cis* generated from photoinduced isomerization during a course of 2 h of experiments was negligible. Identical steady-state spectra of both *trans* and *cis* were measured with samples before and after experiments, implying that photoexcitation of 4TCE did not produce any additional photoproducts.

2.2. Transient Absorption (TA). Our experimental setup has been described in detail elsewhere;[38,39] here we briefly note important features of the setup that are critical for the experiments described in this work. Ultrafast light pulses used in these measurements were generated with a regeneratively amplified Ti:sapphire laser system (Coherent Legend Elite, 1 kHz rep. rate, 35 fs pulse duration, 4.0 mJ/pulse). Tunable excitation pulses were generated with an optical parametric amplifier (OPA, Coherent Operasolo), either through fourth-harmonic generation of the OPA signal (350−380 nm), fourth harmonic generation of the idler (420−460 nm) or sum-frequency of the signal (470−530 nm); 400 nm excitation pulses were generated via second-harmonic generation of the laser fundamental. Broadband probing continua (400−740 nm) were obtained by white-light generation in a 2 mm calcium fluoride (CaF_2) plate. Pulse energies for all actinic pump wavelengths were attenuated to about 1 μJ/pulse for all data presented. In order to eliminate signatures of time-dependent polarization anisotropy from the measured dynamics, the polarization of the white-light probe was set at the magic angle relative to the polarization of the actinic pump using a thin broadband wire-grid polarizer (Thorlabs) placed immediately before the sample. Probe pulses were focused to a spot size at the sample of 50 μm using an off-axis parabolic reflector; the pump beam was focused to a size of <100 μm and was overlapped with the probe beam at a small angle at the sample. The pump pulse delay relative to the probe pulse was controlled with a motorized translation stage (Newport), outfitted with a corner-cube mirror. Probe light transmitted through the sample was filtered and dispersed onto a multichannel array, and transient spectra were calculated using an acquisition algorithm described in the Supporting Information.

2.3. Computational. Calculations using the Gaussian 09 package[40] were performed at the CAM-B3LYP/6-31G* level and utilized Polarizable Continuum Model (PCM) to incorporate the effect of

DOI: 10.1021/jacs.5b07348
J. Am. Chem. Soc. 2015, 137, 10841−10850

solvent (chlorobenzene). All geometry optimizations were carried out without symmetry constraints. Vibrational analysis at the optimized geometries returned no imaginary frequencies. Relaxed potential-energy surfaces (PES) for the S_0 and T_1 states were performed by scanning the central ethylene dihedral angle between 0 and 180 deg in 10 deg/step and optimizing the structure at each step. Time-dependent density functional theory (TD-DFT) was used to determine the energies of geometry-relaxed S_1 states and vertical electronic transition energies from the S_0 and T_1 states. Natural transition orbital (NTO) analysis was employed to assign the transition type. Spin−orbital constants (SOC) were calculated using the Breit−Pauli operator[41] in QChem 4.2.

3. EXPERIMENTAL RESULTS

3.1. Photoinduced Dynamics of *trans*-4TCE. *3.1.1. Low-Energy Excitation of trans-4TCE (530 nm).* Figure 2(a) shows time-resolved TA spectra of *trans*-4TCE following its excitation at 530 nm. At early time delays the spectra consist of negative and positive intensities below and above 655 nm, respectively. Transient features are observed to decay over the few hundred picoseconds that follow excitation. In addition, the negative spectral intensity below 650 nm is observed to bifurcate on a time scale of ∼10 ps. The bluer region of the negative features can be assigned to ground-state bleach (GSB) of *trans*-4TCE because it overlaps with the intense, lowest-energy band in the steady-state absorption spectrum of this isomer. Negative spectral intensity appearing at lower energies (∼600 nm) therefore correspond with stimulated emission (SE) from the lowest-lying singlet excited state, as it matches the position of the steady-state fluorescence spectrum. The SE band and the positive signal above 655 nm share similar decay dynamics, and we can therefore attribute the latter to the excited-state transient absorption of the excited state (singlet transient absorption, or STA). At relatively long time delays (e.g., 464 ps in Figure 2(a)) only a permanent bleach remains between 475 and 550 nm, the shape of which matches the UV−vis difference spectrum between *cis*- and *trans*-4TCE.

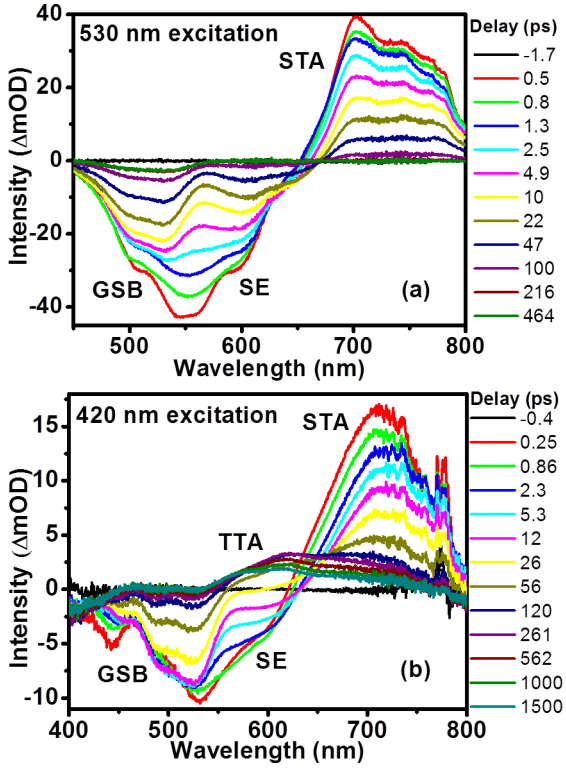

Figure 2. Transient absorption (TA) spectra of *trans*-4TCE in chlorobenzene excited at (a) 530 nm and (b) 420 nm. (a) Spectral evolution is characterized by decay of all three signals (GSB, SE, and STA) within 500 ps. A permanent GSB signal persists on longer time scales, reflecting that a fraction (11.6%) of the excited state population isomerizes. (b) Spectral evolution is similar to that observed after 530 nm excitation at delays earlier than 20 ps, but exhibits signatures of triplet absorption on longer time scales.

Single-wavelength traces at 510, 600, and 740 nm reflect the time-dependence of the GSB, SE and STA, respectively, and were used to characterize quantitatively the relaxation kinetics that follow excitation of *trans*-4TCE at 530 nm; these transients are plotted in Figure S2, with fitting parameters tabulated in Table 1. The 510 nm transient is fit well by a single-exponential decay with a 39.2 ps lifetime. In contrast the SE and STA intensities both exhibit an additional fast decay component, such that a biexponential kinetic model is necessary to fit these traces accurately, with decay time scales of $\tau_1 \approx 2-3$ ps and $\tau_2 \approx 38$ ps. As GSB recovery only occurs on the longer of these time scales, the spectral dynamics of both the SE and STA bands must reflect ultrafast relaxation in the excited state. This assignment is corroborated by the observation of a fast shift in the SE band position, which reflects evolution in S_0-S_1 vertical energy gap between the Franck−Condon region and the excited-state minimum; characterization of this shift in SE is described in the Supporting Information. A global fit of spectral dynamics starting from 10 ps (after excited-state relaxation is complete) returns a 40.0 ps lifetime for the first excited state.

Table 1. Lifetimes from Best-Fit Decay Models for 4TCE Excited at 420 and 530 nm

isomer	excitation λ (nm)	fitting content[a]	τ_1 (ps)	τ_2 (ps)
trans	530	510 nm (GSB)		39.2
		600 nm (SE)	2.3	37.0
		740 nm (STA)	2.9	38.6
		red shift of SE	7.0	
		global fit to decay of all species[b]		40.0
	420	red shift of SE	4.5	
		SE intensity decease	4.3	
		global fit of STA to TTA conversion[c]		40.0
cis	530	452 nm (STA 2)	4.8	
		700 nm (STA 1)	0.38	17.1
	420	472 nm (STA 2)	3.6	
		global fit of TTA to *trans* S_0 conversion[d]		396

[a]Wavelengths designate specific time-dependent cuts through transients. [b]Global fitting was applied to all transients at times >10 ps. [c]Global fitting was applied to all transients between 10 and 215 ps. [d]Global fitting was applied to all transients between 316 and 1500 ps.

The transient data shown in Figures 2(a) and S2 can be used to assess directly the quantum yield for *trans*-to-*cis* isomerization of *trans*-4TCE excited at 530 nm: On the basis of the decay and offset amplitudes of the exponential fit applied to the bleach data (Figure S2), we find that 88.4% of the excited population of *trans*-4TCE returns to its ground state. This indicates an 11.6 ± 1.4% *trans*-to-*cis* isomerization yield at 530 nm, assuming that there are no additional excited-state deactivation/isomerization pathways. A distinct *cis* STA is either absent or not resolved in the TA spectral progression, reflecting that isomerization involves a direct nonradiative

DOI: 10.1021/jacs.5b07348
J. Am. Chem. Soc. 2015, 137, 10841−10850

transition (S_1-to-S_0) from *trans* to *cis* or that both isomers have similar STA bands after 10 ps (vide infra).

3.1.2. High-Energy Excitation of trans-4TCE (420 nm). TA spectra of *trans*-4TCE excited at 420 nm are displayed in Figure 2(b). At early time delays (<10 ps) there is strong resemblance to the spectral evolution observed upon excitation at 530 nm: Delays earlier than 10 ps exhibit fast spectral dynamics associated with the nuclear relaxation of the singlet excited state. An analysis similar to that described above was used to isolate SE spectral dynamics, and the ultrafast red shift and intensity decay of the SE region were found to occur with lifetimes of 4.5 (Figure S4(b)) and 4.3 ps (Figure S4(c)), respectively.

Despite similarities with the dynamics observed with lower excitation energies, a new, broad feature centered near 620 nm emerges concurrently with the decay of the STA signal on longer time scales when *trans*-4TCE is excited at 420 nm. On the basis of similarity to the photoinduced absorption spectra of related oligothiophenes at similar time delays following photoexcitation,[30,42,43] we ascribe this broad feature to a triplet transient absorption (TTA, $T_1 \rightarrow T_N$) of 4TCE. Excited-state decay by way of ISC therefore is apparent from an isosbestic point at 665 nm that appears between 10 and 215 ps. A global kinetic analysis of spectra collected between these delays reveals that the relaxed singlet excited state has a 40.0 ps lifetime (Figure S5) as a result of competing ISC and partial GSB recovery (i.e., internal conversion, IC). After 215 ps the TTA signal decays slightly and by 1500 ps the long-lived signal is a combination of TTA and GSB. On even longer time scales (up to 5.5 ns) the TTA intensity and the GSB intensity do not change noticeably (Figure S9(a)).

Spectral dynamics observed following 530 and 420 nm excitation of *trans*-4TCE are representative of two distinct excited-state relaxation behaviors; a transition between these two behaviors is observed as the pump pulse is tuned from the visible to the near UV, as illustrated in Figure S10.

3.2. Photoinduced Dynamics of *cis*-4TCE. *3.2.1. Low-Energy Excitation of cis-4TCE (530 nm).* Figure 3(a) shows the TA spectra of *cis*-4TCE following 530 nm excitation. The position of most spectral features are similar to those observed for the *trans* isomer, with evidence for ground-state bleaching below 575 nm, stimulated emission near 600 nm, and excited-state absorption above 650 nm. In addition, a second intense excited-state absorption band appears below 475 nm (STA 2), and overlaps significantly with the region where we anticipate the appearance of *cis*-4TCE GSB.

Spectra collected at early delays (t = 0.8 to 5.0 ps) reveal a blue shift as well as a rapid decay of STA 2. Additionally, the STA1 and GSB/SE features are observed to decay much more significantly during the first 10 ps than what is observed for *trans*-4TCE. All transient features decay within 300 ps. Fitting the intensity decay of STA1 at a single wavelength (700 nm) to a biexponential model gives two time scales: 0.38 and 17.1 ps (Figure S7). A single exponential fit of the 452 nm trace gives a 4.8 ps decay constant (Figure S6); the SE band, which is partially overlapped with the lower-energy absorption band, STA 1, undergoes a red shift from 580 to 620 nm on a similar time scale. In total, the ultrafast spectral relaxation of *cis*-4TCE occurs on somewhat faster time scales than observed for relaxation of the *trans* isomer at the same pump wavelength. However, only a very small permanent bleach (<~2% compared to the initial GSB intensity) persists at long time delays for the *cis* isomer, meaning that photoinduced

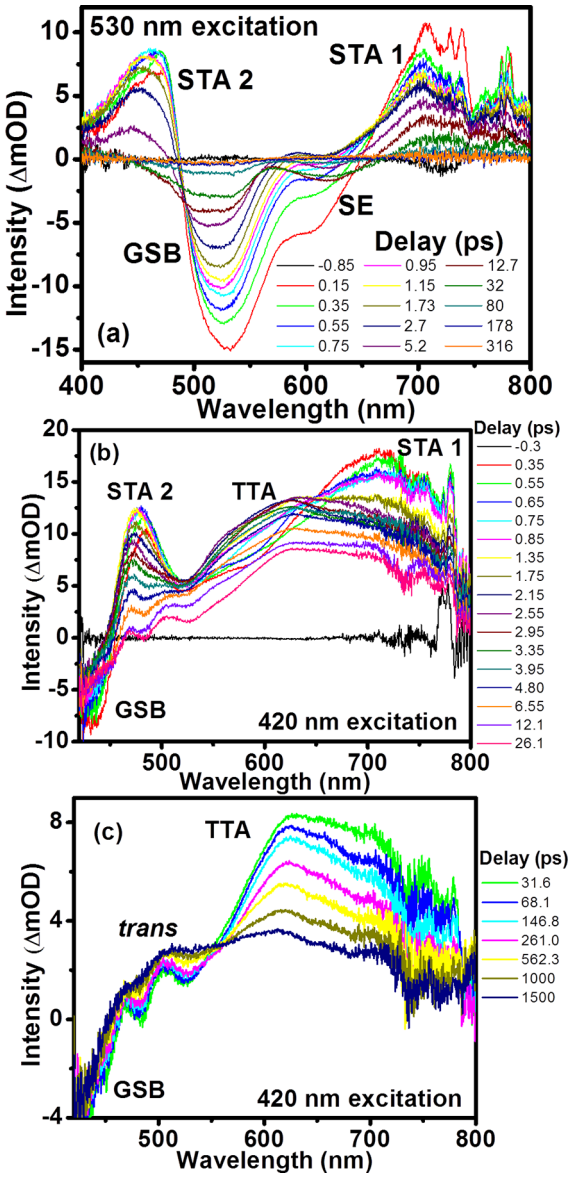

Figure 3. (a) TA spectra of *cis*-4TCE in chlorobenzene following 530 nm excitation: Spectral dynamics are similar to those observed for the *trans* isomer, but exhibit negligible signatures of isomerization. TA spectra of *cis*-4TCE in chlorobenzene (b) ~0−30 ps and (c) after 30−1500 ps after excitation at 420 nm. (b) Ultrafast ISC occurs in the first 2 ps, with a decay of STA 1 at 720 nm and an appearance of TTA at 620 nm. (c) From 30 to 1500 ps the intensity of TTA is substantially reduced, while absorption of the S_0 *trans* isomer concurrently appears between 450 and 560 nm. This *cis*-to-*trans* ISC is evidenced by the isosbestic point at 556 nm.

isomerization is considerably less favored at 530 nm excitation relative to the *trans* isomer.

3.2.2. High-Energy Excitation (420 nm). TA spectra of *cis*-4TCE excited at 420 nm are presented in Figure 3(b) and 3(c). Transient spectra collected at early time delays (Figure 3(b)) are characterized by a broad, intense excited-state absorption (STA 1) peaking at 720 nm and a narrow positive feature at higher energies (475 nm, STA 2); these features are similar to those observed with 530 nm excitation, but obscure the negative GSB and SE signals anticipated between 500 and 600 nm (although GSB can be seen below 450 nm).

DOI: 10.1021/jacs.5b07348
J. Am. Chem. Soc. 2015, 137, 10841−10850

Spectral dynamics during the first 26 ps can be explained as follows: Absorption around 720 nm (STA 1) undergoes a fast decay with concomitant appearance of a feature centered at 620 nm within the first 2 ps. The shape and peak position of the resultant spectrum is similar to what is observed following ISC of excited *trans*-4TCE and small oligothiophenes, indicating that high-energy excitation of *cis*-4TCE likewise leads to ISC, but on a considerably faster time scale. The assignment of this dynamic to ultrafast ISC is supported by the appearance of a quasi-isosbestic point near 665 nm. Meanwhile, STA 2 exhibits a rapid decay, similar to what is observed following excitation at 530 nm, with the peak position of STA 2 red shifting to 472 nm in the first few hundred femtoseconds. By fitting the 472 nm trace intensity with a single exponential decay function, we obtain a decay lifetime of 3.6 ps (Figure S6). By 12 ps STA 2 has vanished, leaving the broad absorption above and a negative GSB below 450 nm. On a similar time scale the absorption between 460 and 800 nm exhibits a slight decay in intensity.

Over the next nanosecond (Figure 3(c)) the absorption band peaking at 620 nm decays significantly, while the spectral intensity between 466 and 556 nm increases. An isosbestic point appears at 556 nm during this time regime, implying that the nascent triplet relaxes to yet another state. As the spectrum of *trans*-4TCE (Figure 1) and its difference spectrum with the *cis* isomer (Figure S10) peak between 450 and 560 nm, the intensity increase below the isosbestic point indicates the formation of the ground-state *trans* isomer through ISC from the T_1 state. A global fit with a sequential two-state kinetic model from 30 to 1500 ps reveals a 0.4 ns time scale for this process (Figure S8). By 1500 ps the transient spectrum includes TTA absorption overlapped with the residual GSB below 450 nm and the absorption from the newly formed S_0 *trans*-4TCE. Nanosecond measurements up to 5.5 ns (Figure S9(b)) reveals similar evolution as observed with *trans*-4TCE and no GSB recovery on this longer time scale.

Spectral dynamics observed following excitation at intermediate wavelengths exhibit a combination of the spectral dynamics observed with 420 and 530 nm, as illustrated in Figure S11. Only excitation wavelengths shorter than 440 nm produce the long-lived TTA and GSB signals apparent in Figure 3, indicating that some portion of the excited *cis* molecules have transferred into the triplet manifold at this energy and are unable to internally convert to the *cis* ground-state. This roughly matches the onset wavelength we previously observed for *cis*-to-*trans* photoconversion to a photostationary state.

3.3. Triplet-Sensitized Energy Transfer. In order to verify that *cis*-to-*trans* isomerization occurs via the triplet manifold, we used methylene blue (MB, $\Phi_{ISC} = 0.52$)[44] as a sensitizer to prepare T_1 4TCE. These measurements were conducted with 4TCE in acetonitrile, as MB has poor solubility in CB. The steady-state UV−vis absorption of MB is most intense at 650 nm, which lies at significantly lower energy than the lowest-energy absorption band of either *trans*- or *cis*-4TCE. Furthermore, the T_1−S_0 energy gap of both 4TCE isomers is calculated to be lower than that of MB (Table 2). Therefore, we expect that effective triplet energy transfer from MB to 4TCE is possible for both isomers.

Experimentally, a mixture of *cis*-4TCE and MB in acetonitrile (not deoxygenated) was exposed to 650 nm light. Within 8 min isomerization from *cis* to *trans* was clearly observed via steady-state UV−vis spectroscopy, as evidenced by the appearance of an isosbestic point at 435 nm (Figure 4(a)). The intensity of

Table 2. Experimental and Calculated Energies of S_0−S_1 and S_0−T_1 Energy Gaps for 4TCE and MB (Unit: eV)

	S_0−S_1 (exp.)	S_0−S_1 (calc.)[a]	S_0−T_1 (exp.)	S_0−T_1 (calc.)[a]
cis-4TCE[b]	2.64	2.86		1.27
trans-4TCE[b]	2.38	2.60		1.11
MB	1.89[b]/1.86[c]		1.43[c]	

[a]Vertical excitation energy calculation (TD-DFT/CAM-B3LYP/6-31G*/PCM). [b]From UV−vis spectrum in acetonitrile. [c]"In polar solvent", taken from ref 44.

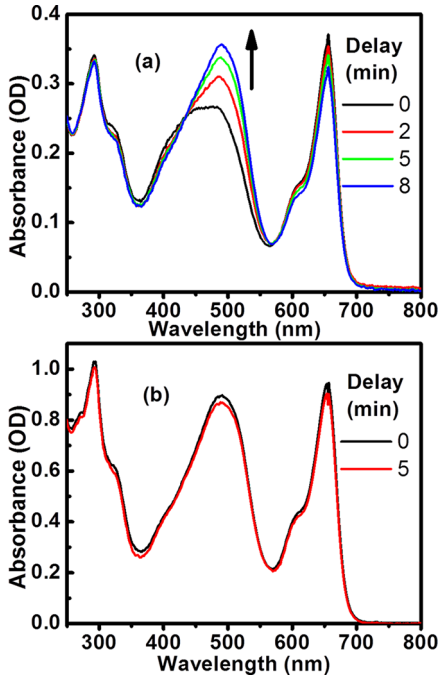

Figure 4. Evolution of UV−vis spectra recorded during 650 nm light illumination (I = 2.6 mW) of (a) *cis*-4TCE ($c = 2.2 \times 10^{-5}$ M) and methylene blue (MB, $c = 4.6 \times 10^{-6}$ M) and (b) *trans*-4TCE ($c = 3.2 \times 10^{-5}$ M) and MB ($c = 1.2 \times 10^{-5}$ M) in acetonitrile. Neither solution was degassed.

MB absorption centered at 650 nm was also observed to decrease, most likely the result of some oxidation of MB in solution. Triplet sensitization of the isomerization of *trans*-4TCE was attempted in the same way, but no spectral change associated with *trans*-to-*cis* isomerization was observed upon 650 nm radiation (Figure 4(b)).

3.4. Computational Results. We previously reported that the *trans* isomer is ca. 4 kcal/mol more energetically stable than *cis*-4TCE; the relative stability of *cis* over *trans* under room-light illumination is related to the relative intensities and positions of their respective steady-state absorption features, as well as the relative quantum yields for photoisomerization with visible light. The calculated vertical transition to the S_1 state is 2.60 eV (oscillator strength f = 1.43) for *trans* and 2.86 eV (f = 0.67) for *cis*. The difference in calculated transition energies for the two isomers (0.26 eV) matches the differences measured experimentally (also 0.26 eV). Furthermore, the ratio of calculated oscillator strengths (2.13) are also in reasonable accord with experiment (2.4 based on peak intensities). This disparity in oscillator strength means that *trans* can more effectively absorb visible light.

DOI: 10.1021/jacs.5b07348
J. Am. Chem. Soc. 2015, 137, 10841−10850

In the TA spectra for both *trans* and *cis* the SE peaks near 600 nm. The SE peak reflects the vertical energy gap from the first excited state back to the ground state. Stationary minima were located for the S_1 state of both isomers and calculated energies are collected in Table S1. During the relaxation of the *trans* isomer in the first excited state, elongation of the ethylene bond length from 1.373 to 1.447 Å and increase of the central dihedral angle θ (C(cyano)−C(et)−C(et)−C(cyano)) to 36° render an energy decrease by 0.44 eV. Similarly in *cis*, the ethylene bond length alters from 1.366 to 1.452 Å and θ changes from 175° to 139° with a 0.77 eV energy decrease during the relaxation. Accordingly, the S_0−S_1 gap shrinks, giving rise to the red shift of SE observed in the TA spectra. This relaxation may also alter the S_1−S_n gaps as well, and likely explains the time-dependence in the STA2 position for *cis*-4TCE. The calculated energy gap between the Franck−Condon region (S_1*) and S_1 minimum is in qualitative accord with the observation of spectral relaxation of SE observed for both isomers.

TD-DFT calculations were used to predict the higher-lying bright states in the singlet manifold: S_6 (f = 0.43) for *trans*, S_2 (f = 0.50) and S_4 (f = 0.17) for *cis* (Figure 5). TD-DFT

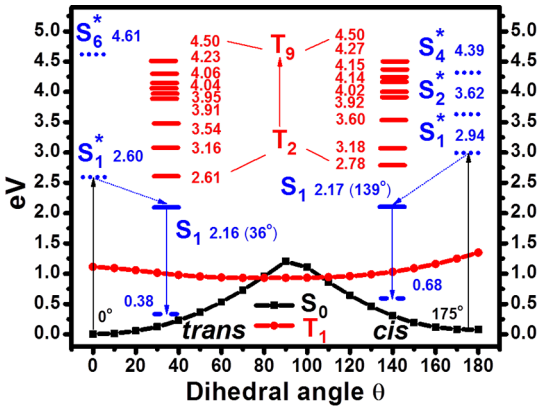

Figure 5. Diagram of calculated state energies for 4TCE. Energies of singlet excited states are evaluated at the optimized ground-state geometry. The S_1 geometries of both isomers were also optimized; high-lying triplet levels were calculated from the S_1 minimum geometries. Although isomerization likely involves multiple coordinates, the dihedral angle of the central ethylene is anticipated to be most significant. Relaxed PES scans of S_0 and T_1 were performed in steps of 10 deg. These two potential curves intersect near θ = 90°.

calculations also predict the relative position and intensity of TTA signals: For the *trans* isomer the strongest absorption is $T_1 \rightarrow T_3$ at 578 nm (f = 1.19), and in *cis* it is $T_1 \rightarrow T_3$ at 571 nm (f = 0.43); these are in close agreement with the features assigned to TTA from experimental measurements. In order to explore the density of triplet levels relevant at various excitation energies, the energies of various triplet states were calculated at the S_1 equilibrium geometry; 8 and 7 triplet excited states were found to lay between S_1/S_6 for *trans*- and S_1/S_4 for *cis*-4TCE, respectively.

In order to better understand why isomerization might proceed via the T_1 level, we also carried out relaxed PES scans of the S_0 and T_1 states; the results are plotted in Figure 5. Most importantly, these two potential curves intersect near θ = 90°. The PES of S_0 exhibits a 1.2 eV barrier at the perpendicular geometry, while the T_1 surface is found to be barrierless from the Franck−Condon region to the S_0/T_1 crossing along this particular coordinate. Notably, the relaxed T_1 PES slightly favors (is flatter toward) smaller dihedral angles, closer to the *trans* well of the S_0 surface.

4. DISCUSSION

4.1. Energy-Dependent Relaxation Pathways and Photoswitching Mechanisms. On the basis of the spectral dynamics presented above, we summarize the excited-state relaxation following 530 nm photoexcitation as shown in Figure 6(a): Excitation of *trans*-4TCE to its S_1 state at this wavelength

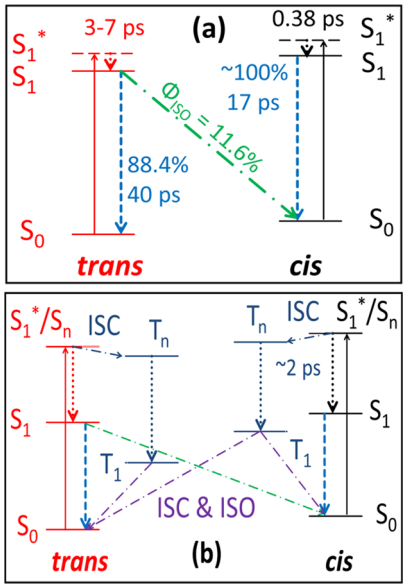

Figure 6. Schematic of isomerization pathways for 4TCE excited at (a) 530 nm and (b) 420 nm. For 530 nm excitation 11.6% of S_1 *trans* isomer undergoes isomerization to *cis*. For 420 nm excitation the relaxation for both isomers occurs through the triplet manifold. Ultrafast ISC (~2 ps) occurs in *cis*-4TCE, and *cis*-to-*trans* isomerization (ISO) occurs through the T_1/S_0 coupling on a time scale of 0.4 ns.

results in excited-state relaxation on a time scale of 3−7 ps; this is followed by S_1 decay on a time scale of 40 ps that returns 88% of the excited-state population to S_0 *trans*-4TCE while the remaining 12% isomerizes to S_0 *cis*-4TCE.

Excitation of *cis*-4TCE at 530 nm is likewise followed by excited-state relaxation on a time scale of a few picoseconds. The rapid decrease of the ground-state bleach on the time scale associated with nuclear relaxation of the excited state indicates that internal conversion back to the ground state is highly structure dependent. In total, S_1 *cis*-4TCE decays via internal conversion to the *cis* ground state, with virtually no isomerization to *trans*-4TCE (<2%).

Excited-state relaxation pathways following excitation at 420 nm are shown schematically in Figure 6(b) for both isomers. Excitation of *trans*-4TCE at this energy results in population of S_1 with considerable excess vibrational energy. Excited-state relaxation occurs on a time scale of 3−7 ps, similar to what is observed at lower energies. This is followed by excited-state decay on a time scale of 40 ps that results in a partial recovery of the *trans* ground state as well as intersystem crossing into the triplet manifold of 4TCE. We see no evidence for *trans*-to-*cis* isomerization from time-resolved measurements up to 5.5 ns. We note that this time scale is considerably longer than time scales for vibrational energy relaxation and transfer in solution,

DOI: 10.1021/jacs.5b07348
J. Am. Chem. Soc. 2015, 137, 10841−10850

and therefore the triplet spectrum observed corresponds with a relaxed T_1. Triplet sensitizer measurements further suggest that isomerization only occurs via the singlet manifold for *trans*-4TCE. As both excitation pathways are expected to create T_1 with relatively little excess internal energy, we take both pieces of data to imply that *trans*-to-*cis* isomerization does not occur by way of the triplet manifold.

Excitation of *cis*-4TCE at the same energy reveals that a significant fraction of the population of photoexcited molecules undergoes ultrafast (~2 ps) intersystem crossing into the triplet manifold, with the remaining singlet excited 4TCE relaxing in a manner similar to *cis*-4TCE excited at 530 nm. A fraction of the triplet population relaxes to S_0 *trans*-4TCE on a 400 ps time scale, with the remaining triplet population persisting beyond 5 ns.

This interpretation of photophysical relaxation pathways based on our ultrafast spectral measurements is highly consistent with the wavelength-dependent isomerization yields observed for 4TCE. The following equation reflects the relationships that controls photoconversion,[45]

$$\frac{[t]}{[c]} = \frac{Y^{ct} \times \varepsilon_c}{Y^{tc} \times \varepsilon_t}$$

where $[t]$ and $[c]$ denote the concentration of *trans* and *cis* in the photostationary state (PSS), Y^{ct} and Y^{tc} are the quantum yields for the *cis*-to-*trans* and *trans*-to-*cis* isomerization reaction, respectively, and the extinction coefficients of *cis* and *trans* are represented by ε_c and ε_t. Thus, at 530 nm pump wavelength Y^{ct} is <2% while Y^{tc} = 11.6 ± 1.4%, meaning that the photoisomerization from *trans* to *cis* proceeds with nearly 100% efficiency. Meanwhile, the reverse reaction can be triggered by pumping at 420 nm; at this wavelength $\varepsilon_c/\varepsilon_t$ = 1.6 and Y^{ct} and Y^{tc} are estimated as 4.68 ± 0.24% and 23.0 ± 1.5%, respectively (see Supporting Information). Relaxation of *cis*-4TCE by way of the triplet manifold therefore enables *cis*-to-*trans* isomerization with a large enough quantum yield to enable the buildup of a significant concentration of *trans*-4TCE at the PSS. We note, however, that the photostationary yields obtained are solvent dependent (0.3 for CB, 0.6 for toluene), which reflects differences in the relative stabilization of singlet vs triplet levels that affect the ISC dynamics into and out of the triplet manifold.[46−48] Further work is underway to interrogate this solvent-dependent effect, as it represents a means for controlling relative isomerization yields and switch performance.

4.2. Photoisomerization of 4TCE through the Triplet Manifold. *4.2.1. Singlet-to-Triplet Intersystem Crossing in 4TCE.* It is well-known that short oligothiophenes have relatively fast ISC kinetics,[30−35] primarily due to the large spin−orbit coupling (SOC) induced by sulfur atoms. Large SOCs also can be expected for excited 4TCE, such that ISC will to be an important photophysical relaxation pathway for 4TCE. An important question regarding ISC relaxation is what gateway states are critical for quickly relaxing between the singlet and triplet manifolds. NTO analysis reveals that S_1, T_{1-2} for both isomers evaluated at the optimized S_1 geometries, and S_6 (*trans*), S_2 and S_4 (*cis*) evaluated at the optimized S_0 geometries all exhibit $\pi-\pi^*$ character (see Supporting Information). Therefore, ISC from the S_1 level to these triplet states are less likely according to the El-Sayed rule.[49] This is in excellent agreement with our experimental findings that no triplet signals were observed at long time delays when pumping at the red side of the low energy absorption bands (530 nm). Higher-lying excited states are rather complicated and higher-level theoretical calculations are required to better understand the ultrafast ISC pathways that contribute following excitation at higher energies. Nonetheless, triplet excited states with large SOC are found 1.5−2.5 eV above the lowest singlet excited state in related oligothiophenes.[50] Additionally, these triplet states have been assigned as quasi-pure $\pi-\sigma^*$ excitations that can enable efficient ISC in heterocyclic compounds.[51,52] We infer that a similar situation exists for photoexcited 4TCE, and would thus facilitate ISC when 4TCE is pumped into higher-lying singlet excited state(s) that are energetically close to triplet states with quasi-pure $\pi-\sigma^*$ character. Wavelength-dependent transient absorption spectra collected at 1 ns for *trans* and 316 ps for *cis* strongly support this hypothesis (Figures S10 and S11(b), respectively).

The fact that *cis*-4TCE exhibits a larger ISC rate than the *trans* isomer can be rationalized through comparisons with oligothiophenes of various lengths. By comparing the photodetachment spectroscopy of oligothiophene anions with the phosphorescence and STA of bi- (2T), ter- (3T) and quarter- (4T) thiophene, Rentsch et al. determined that the relative positions of the S_1 and high-lying triplet levels underlie the extremely high ISC rate observed for 2T when excited to the lowest singlet excited state and the decrease in this rate with increase in oligomer.[34] Beljonne et al. argued that lengthening an oligothiophene should decrease the SOC, since it could enlarge the energetic separation between the π and σ electronic structures and consequently reduce spin−orbit interactions.[50] The effective conjugation length in *cis*-4TCE must be shorter than that in *trans*, as a result of its highly nonplanar configuration; therefore, *cis* is more similar to smaller oligothiophenes (e.g., 2T or 3T), whereas *trans* is analogous to longer oligothiophenes (e.g., 4T or 5T). As a result, *cis* could be expected to have a higher ISC rate, as observed via 420 nm photoexcitation. Similarly, the ultrafast ISC (~2 ps) as well as the trend between pump energy and the triplet quantum yield in *cis*-4TCE is highly similar to what has been observed with 2T and 3T.[33,35] Paa et al. associated the ultrafast ISC of 3T on a ~2 ps time scale to the excited-state structural relaxation, as ISC is more favorable from the unrelaxed, nonplanar excited vibronic singlet state. The triplet yield for 3T, as well as the 2 ps ultrafast decay component, becomes more prominent when the pump energy increases.[33,35] This is similar to what we observe for *cis*-4TCE. In contrast, *trans*-4TCE exhibits a much slower ISC time scale, which is consistent with the ISC of longer oligothiophenes.

The twisted conformation of *cis*-4TCE plays an important role in promoting ultrafast ISC, and therefore points to a structure-dynamics relationship that critically underlies the *cis*-to-*trans* isomerization pathway of this photoswitch. According to the symmetry selection rules for ISC, lower symmetry of an oligothiophene can strongly increase the SOC.[50] The planar conformation of the *trans* isomer can largely enhance the S_0-S_1 transition in the visible region, but would also impede ISC, even if the conjugated backbone contains heavy atoms. As a result, while longer effective conjugation length is attractive for the design of 4TCE derivatives because it can push the absorption transition that enables *trans*-to-*cis* isomerization further into the red, intramolecular interactions that maintain an effectively shorter conjugation length should be concurrently maintained in order to promote the reverse isomerization

DOI: 10.1021/jacs.5b07348
J. Am. Chem. Soc. 2015, 137, 10841−10850

through excitation at higher energies to enable efficient ISC into the triplet manifold.

4.2.2. Triplet Isomerization of cis-4TCE. As with oligothiophenes, it can be presumed that 4TCE will undergo fast internal conversion through the dense manifold of triplet states once it crosses into the triplet manifold, quickly relaxing to the T_1 state. Isomerization or ground-state recovery must then occur via ISC from the lowest triplet level. The relaxed PES scan along the θ coordinate (Figure 5) indicates that the PES of T_1 has a flat minimum that is nearly perpendicular and slightly favors a configuration that falls within the *trans* ground-state well. Although the photoinduced excited-state dynamics need not follow this calculated pathway exactly, this observation helps to explain the observation of *cis*-to-*trans* but not *trans*-to-*cis* isomerization by way of triplet manifold. The T_1 PES also crosses the S_0 surface at nearly perpendicular geometries, which should greatly enhance the probability for isomerization via ISC when an excited-state wave function or wavepacket is able to approach the crossing. In fact, the T_1/S_0 SOC calculated at the $\theta = 90$ geometry has a substantial value of 59.83 cm^{-1}, which is significantly larger than those of planar aromatic compounds (typically less than 1 cm^{-1}).[53] Therefore, it is conceivable that T_1 4TCE could readily return to the singlet manifold through ISC on a sub-ns time scale.[54,55]

The conclusion that *cis*-to-*trans* photoisomerization occurs by way of the triplet manifold (whereas *trans*-to-*cis* isomerization does not) is further corroborated by triplet energy-transfer experiments. Conspicuously, excitation of MB at 650 nm induces *cis*-4TCE to isomerize, whereas the reverse isomerization under the same condition is not observed. More detailed interrogation with regards to the type and relative concentration of triplet sensitizer is certainly necessary to elucidate the generality of the triplet sensitization of 4TCE. However, sensitizer experiments raise interesting possibilities for future molecular design or applications with 4TCE derivatives: Specifically, one could conceivably combine the isomerizing moiety with a sensitizing group; this could enable shifting the wavelengths for *cis* to *trans* isomerization into redder spectral regions (Figure 4).[56,57] As demonstrated with MB, the triplet energy transfer to *cis*-4TCE is highly effective and far more photoselective that direct excitation of this isomer at bluer wavelengths: The formation of the *trans* isomer can be detected within a few minutes of radiation with 650 nm light, even in the presence of oxygen; this is similar to the time scale necessary to reach the PSS via direct excitation at 420 nm. Although the presence of oxygen has the potential to quench excited triplet sensitizers, we expect that *cis* to *trans* isomerization itself is efficient following energy transfer because isomerization is complete within a nanosecond, as observed following photoexcitation of *cis*-4TCE at 420 nm.

5. CONCLUSIONS

4TCE is an attractive switch for applications that require *E*/*Z* isomerization upon visible light irradiation and also exhibits an interesting and potentially exploitable exclusivity in its forward and reverse photoisomerization mechanisms: Upon photoexcitation with wavelengths longer than 460 nm, isomerization in 4TCE occurs exclusively from *trans* to *cis* and only involves electronic relaxation within the singlet manifold. In contrast, *cis*-to-*trans* isomerization can be achieved by irradiation at wavelengths <460 nm, whereby the photoprepared state undergoes fast ISC into the triplet manifold and then isomerizes from the lowest triplet level within 1 ns; this pathway is possible due to large spin−orbit coupling common to short oligothiophenes and thiophene-based systems. In addition, triplet energy-transfer can be used to induce *cis* to *trans* isomerization, but not the reverse. Thus, the switching state can be selectively controlled by illumination at different visible wavelengths, but can also be selectively discriminated through indirect sensitization.

This separation of isomerization mechanisms between manifolds of different multiplicity has important implications for tailoring switch design: For instance, elongation of the effective conjugation of 4TCE derivatives by lengthening the pendant oligothienyl groups is an intriguing strategy for generating *E*/*Z* photoswitches that operate at even longer wavelengths. However, this design strategy must also take into consideration how the fast ISC process underlying the *cis*-to-*trans* isomerization pathway is altered with increased conjugation length; notably, related oligothiophenes exhibit slower ISC rates with increasing conjugation length. Therefore, it may be necessary to introduce a slightly twisted torsional conformation between thiophene rings through the addition of pendant substituents in order to maintain an efficient, ultrafast ISC[58] while increasing the length of the pendant oligothienyl groups. Alternatively, elongation of the oligothienyl groups could be used to squelch *cis*-to-*trans* photoisomerization, enabling unidirectional light-activated structural changes, as may be desired for the preparation of spatially patterned material morphologies. This separation of forward and reverse isomerization pathways could also lend itself to control with variation in chemical or physical environment (e.g., variations in solvent/matrix properties or presence of electric fields). Finally, incorporation of a triplet-sensitizing moiety into 4TCE derivatives has the potential to improve the selectivity of *cis* to *trans* isomerization, accompanied by a substantial red shift of the corresponding isomerization wavelength. As demonstrated here, the efficacy of all of these possibilities rests on the structure-dynamics relationships that control the photophysical dynamics underlying each photoisomerization mechanism.

■ ASSOCIATED CONTENT

Supporting Information

The Supporting Information is available free of charge on the ACS Publications website at DOI: 10.1021/jacs.5b07348.

Quantum-yield measurements and actinometry, additional experimental details, TA spectral analysis and kinetic modeling, and additional computational details and outputs from quantum-chemical calculation. (PDF)

■ AUTHOR INFORMATION

Corresponding Author

*artbragg@jhu.edu

Present Address

[§]Dalian National Laboratory for Clean Energy, Dalian Institute of Chemical Physics, Chinese Academy of Sciences, 457 Zhongshan Rd., Dalian 116023, China.

Notes

The authors declare no competing financial interest.

■ ACKNOWLEDGMENTS

Acknowledgement is made to the donors to the ACS Petroleum Research Fund for partial support of this work (A.E.B. and J.Z.). Support from NIOSH Grant 5R21OH010190-02 is also gratefully acknowledged (H.E.K

DOI: 10.1021/jacs.5b07348
J. Am. Chem. Soc. 2015, 137, 10841−10850

and X.G). Computational aspects of this work used resources of NERSC, supported by the U.S. Department of Energy (Contract No. DE-AC02-05CH11231). We thank Qi Ou for calculating the spin−orbit coupling strength and Joshua Snyder for assistance with measurements of nanosecond transient absorption spectra. J. Z. gratefully acknowledges support through the Langmuir-Cresap fellowship.

REFERENCES

(1) Irie, M. *Chem. Rev.* **2000**, *100*, 1685−1716.
(2) Minkin, V. I. *Chem. Rev.* **2004**, *104*, 2751−2776.
(3) Irie, M.; Fukaminato, T.; Matsuda, K.; Kobatake, S. *Chem. Rev.* **2014**, *114*, 12174−12277.
(4) Helmy, S.; Leibfarth, F. A.; Oh, S.; Poelma, J. E.; Hawker, C. J.; Read de Alaniz, J. *J. Am. Chem. Soc.* **2014**, *136*, 8169−8172.
(5) Natansohn, A.; Rochon, P.; Ho, M.-S.; Barrett, C. *Macromolecules* **1995**, *28*, 4179−4183.
(6) Andreasson, J.; Pischel, U.; Straight, S. D.; Moore, T. A.; Moore, A. L.; Gust, D. *J. Am. Chem. Soc.* **2011**, *133*, 11641−11648.
(7) Koumura, N.; Zijlstra, R. W. J.; Delden, R. A. v.; Harada, N.; Feringa, B. L. *Nature* **1999**, *401*, 152−155.
(8) Koumura, N.; Geertsema, E. M.; Meetsma, A.; Feringa, B. L. *J. Am. Chem. Soc.* **2000**, *122*, 12005−12006.
(9) Beharry, A. A.; Woolley, G. A. *Chem. Soc. Rev.* **2011**, *40*, 4422−4437.
(10) Samanta, S.; Qin, C.; Lough, A. J.; Woolley, G. A. *Angew. Chem., Int. Ed.* **2012**, *51*, 6452−6455.
(11) Kamiya, Y.; Asanuma, H. *Acc. Chem. Res.* **2014**, *47*, 1663−1672.
(12) Bandara, H. M.; Burdette, S. C. *Chem. Soc. Rev.* **2012**, *41*, 1809−1825.
(13) Szymanski, W.; Beierle, J. M.; Kistemaker, H. A.; Velema, W. A.; Feringa, B. L. *Chem. Rev.* **2013**, *113*, 6114−6178.
(14) Velema, W. A.; Szymanski, W.; Feringa, B. L. *J. Am. Chem. Soc.* **2014**, *136*, 2178−2191.
(15) Gemayel, M. E.; Borjesson, K.; Herder, M.; Duong, D. T.; Hutchison, J. A.; Ruzie, C.; Schweicher, G.; Salleo, A.; Geerts, Y.; Hecht, S.; Orgiu, E.; Samori, P. *Nat. Commun.* **2015**, *6*, 6330.
(16) Martinez-Lopez, D.; Yu, M. L.; Garcia-Iriepa, C.; Campos, P. J.; Frutos, L. M.; Golen, J. A.; Rasapalli, S.; Sampedro, D. *J. Org. Chem.* **2015**, *80*, 3929−3939.
(17) Leonard, J.; Schapiro, I.; Briand, J.; Fusi, S.; Paccani, R. R.; Olivucci, M.; Haacke, S. *Chem. - Eur. J.* **2012**, *18*, 15296−15304.
(18) Sinicropi, A.; Martin, E.; Ryazantsev, M.; Helbing, J.; Briand, J.; Sharma, D.; Leonard, J.; Haacke, S.; Cannizzo, A.; Chergui, M.; Zanirato, V.; Fusi, S.; Santoro, F.; Basosi, R.; Ferre, N.; Olivucci, M. *Proc. Natl. Acad. Sci. U. S. A.* **2008**, *105*, 17642−17647.
(19) Greb, L.; Lehn, J. M. *J. Am. Chem. Soc.* **2014**, *136*, 13114−13117.
(20) Bonacchi, S.; El Garah, M.; Ciesielski, A.; Herder, M.; Conti, S.; Cecchini, M.; Hecht, S.; Samori, P. *Angew. Chem., Int. Ed.* **2015**, *54*, 4865−4869.
(21) Eelkema, R.; Pollard, M. M.; Katsonis, N.; Vicario, J.; Broer, D. J.; Feringa, B. L. *J. Am. Chem. Soc.* **2006**, *128*, 14397−14407.
(22) Siewertsen, R.; Neumann, H.; Buchheim-Stehn, B.; Herges, R.; Näther, C.; Renth, F.; Temps, F. *J. Am. Chem. Soc.* **2009**, *131*, 15594−15595.
(23) Bleger, D.; Schwarz, J.; Brouwer, A. M.; Hecht, S. *J. Am. Chem. Soc.* **2012**, *134*, 20597−20600.
(24) Herder, M.; Schmidt, B. M.; Grubert, L.; Patzel, M.; Schwarz, J.; Hecht, S. *J. Am. Chem. Soc.* **2015**, *137*, 2738−2747.
(25) Yang, Y.; Hughes, R. P.; Aprahamian, I. *J. Am. Chem. Soc.* **2014**, *136*, 13190−13193.
(26) Yang, Y.; Hughes, R. P.; Aprahamian, I. *J. Am. Chem. Soc.* **2012**, *134*, 15221−15224.
(27) Guo, X.; Zhou, J.; Siegler, M. A.; Bragg, A. E.; Katz, H. E. *Angew. Chem., Int. Ed.* **2015**, *54*, 4782−4786.
(28) Saltiel, J.; Hammond, G. S. *J. Am. Chem. Soc.* **1963**, *85*, 2515−2516.
(29) Herkstroeter, W. G.; Hammond, G. S. *J. Am. Chem. Soc.* **1966**, *88*, 4769−4777.
(30) Grebner, D.; Helbig, M.; Rentsch, S. *J. Phys. Chem.* **1995**, *59*, 16991−16998.
(31) Yang, J.-P.; Paa, W.; Rentsch, S. *Chem. Phys. Lett.* **2000**, *320*, 665−672.
(32) Chosrovian, H.; Rentsch, S.; Grebner, D.; Dahm, D. U.; Birckner, E. *Synth. Met.* **1993**, *60*, 23−26.
(33) Paa, W.; Yang, J.-P.; Helbig, M.; Hein, J.; Rentsch, S. *Chem. Phys. Lett.* **1998**, *292*, 607−614.
(34) Rentsch, S.; Yang, J. P.; Paa, W.; Birckner, E.; Schiedt, J.; Weinkauf, R. *Phys. Chem. Chem. Phys.* **1999**, *1*, 1707−1714.
(35) Paa, W.; Yang, J. P.; Rentsch, S. *Appl. Phys. B: Lasers Opt.* **2000**, *71*, 443−449.
(36) Waldeck, D. H. *Chem. Rev.* **1991**, *91*, 415−436.
(37) Quick, M.; Dobryakov, A. L.; Gerecke, M.; Richter, C.; Berndt, F.; Ioffe, I. N.; Granovsky, A. A.; Mahrwald, R.; Ernsting, N. P.; Kovalenko, S. A. *J. Phys. Chem. B* **2014**, *118*, 8756−8771.
(38) Yu, W.; Zhou, J.; Bragg, A. E. *J. Phys. Chem. Lett.* **2012**, *3*, 1321−1328.
(39) Yu, W.; Donohoo-Vallett, P. J.; Zhou, J.; Bragg, A. E. *J. Chem. Phys.* **2014**, *141*, 044201.
(40) Frisch, M. J.; Trucks, G. W.; Schlegel, H. B.; Scuseria, G. E.; Robb, M. A.; Cheeseman, J. R.; Scalmani, G.; Barone, V.; Mennucci, B.; Petersson, G. A.; Nakatsuji, H.; Caricato, M.; Li, X.; Hratchian, H. P.; Izmaylov, A. F.; Bloino, J.; Zheng, G.; Sonnenberg, J. L.; Hada, M.; Ehara, M.; Toyota, K.; Fukuda, R.; Hasegawa, J.; Ishida, M.; Nakajima, T.; Honda, Y.; Kitao, O.; Nakai, H.; Vreven, T.; Montgomery, J. A.; Peralta, Jr., J. E.; Ogliaro, F.; Bearpark, M.; Heyd, J. J.; Brothers, E.; Kudin, K. N.; Staroverov, V. N.; Kobayashi, R.; Normand, J. ; Raghavachari, K.; Rendell, A.; Burant, J. C.; Iyengar, S. S.; Tomasi, J.; Cossi, M.; Rega, N.; Millam, J. M.; Klene, M.; Knox, J. E.; Cross, J. B.; Bakken, V.; Adamo, C.; Jaramillo, J.; Gomperts, R.; Stratmann, R. E.; Yazyev, O. ; Austin, A. J.; Cammi, R.; Pomelli, C.; Ochterski, J. W.; Martin, R. L.; Morokuma, K.; Zakrzewski, V. G.; Voth, G. A.; Salvador, P.; Dannenberg, J. J.; Dapprich, S.; Daniels, A. D. Farkas, J.; Foresman, B.; Ortiz, J. V.; Cioslowski, J.; Fox, D. J. *Gaussian 09*, Revision A.01; Gaussian, Inc.: Wallingford, CT, 2009.
(41) Nicklass, A.; Peterson, K. A.; Berning, A.; Werner, H.-J.; Knowles, P. J. *J. Chem. Phys.* **2000**, *112*, 5624−5632.
(42) Becker, R. S.; Melo, J. S. d.; Macanita, A. L.; Elisei, F. *J. Phys. Chem.* **1996**, *100*, 18683−18695.
(43) Benincori, T.; Bongiovanni, G.; Botta, C.; Cerullo, G.; Lanzani, G.; Mura, A.; Rossi, L.; Sannicolo, F.; Tubino, R. *Phys. Rev. B: Condens. Matter Mater. Phys.* **1998**, *58*, 9082−9086.
(44) Montalti, M.; Credi, A.; Prodi, L.; Gandolfi, M. T. *Handbook of Photochemistry*; CRC Press: Boca Raton, FL, 2006; pp 601−616.
(45) Fischer, E. *J. Phys. Chem.* **1967**, *71*, 3704−3706.
(46) Barik, A.; Indira Priyadarsini, K. *Spectrochim. Acta, Part A* **2013**, *105*, 267−272.
(47) Hare, P. M.; Crespo-Hernández, C. E.; Kohler, B. *J. Phys. Chem. B* **2006**, *110*, 18641−18650.
(48) Suzuki, K.; Tanabe, H.; Tobita, S.; Shizuka, H. *J. Phys. Chem. A* **1997**, *101*, 4496−4503.
(49) El-Sayed, M. A. *Acc. Chem. Res.* **1968**, *1*, 8−16.
(50) Beljonne, D.; Shuai, Z.; Pourtois, G.; Bredas, J. L. *J. Phys. Chem. A* **2001**, *105*, 3899−3907.
(51) Lower, S. K.; El-Sayed, M. A. *Chem. Rev.* **1965**, *66*, 199−241.
(52) Krishna, V. G.; Goodman, L. *J. Chem. Phys.* **1962**, *37*, 912−915.
(53) Henry, B. H.; Siebrand, W. In *Organic Molecular Photophysis*; Birke, J. B., Ed.; Wiley: London, 1973; Vol. *1*.
(54) Cembran, A.; Bernardi, F.; Garavelli, M.; Gagliardi, L.; Orlandi, G. *J. Am. Chem. Soc.* **2004**, *126*, 3234−3243.
(55) Zhao, H.; Liu, K.; Song, D.; Su, H. *J. Phys. Chem. A* **2014**, *118*, 9105−9112.
(56) Venkataramani, S.; Jana, U.; Dommaschk, M.; Sönnichsen, F. D.; Tuczek, F.; Herges, R. *Science* **2011**, *331*, 445−448.

DOI: 10.1021/jacs.5b07348
J. Am. Chem. Soc. 2015, 137, 10841−10850

(57) Cnossen, A.; Hou, L.; Pollard, M. M.; Wesenhagen, P. V.; Browne, W. R.; Feringa, B. L. *J. Am. Chem. Soc.* **2012**, *134*, 17613−17619.
(58) Zheldakov, I. L.; Wasylenko, J. M.; Elles, C. G. *Phys. Chem. Chem. Phys.* **2012**, *14*, 6211−6218.

DOI: 10.1021/jacs.5b07348
J. Am. Chem. Soc. 2015, 137, 10841−10850